

Contents lists available at ScienceDirect

Journal of Quantitative Spectroscopy & Radiative Transfer

journal homepage: www.elsevier.com/locate/jqsrt



Measurements of the ${}^5D_4^{\circ} - {}^5P_3$ transition of singly ionized atomic iodine using intermodulated laser induced fluorescence



M.I. Lazo^{a,*}, T.E. Steinberger^a, T.N. Good^b, E.E. Scime^a

- ^a West Virginia University, Department of Physics & Astronomy, Morgantown, WV 26506, USA
- ^b Gettysburg College, Department of Physics & Astronomy, Gettysburg, PA 17325, USA

ARTICLE INFO

Article history: Received 16 June 2021 Revised 6 October 2021 Accepted 7 October 2021 Available online 22 October 2021

Keywords: Intermodulated spectroscopy Laser induced fluorescence Singly-ionized atomic iodine Hyperfine structure Hyperfine coupling coefficients

ABSTRACT

lodine has been an element of recent interest for commercial use as fuel in electrostatic propulsion systems. A lingering problem when investigating ionized iodine using non-perturbative, laser-based techniques is determining the spectral width, i.e., the species temperature, of iodine. To this end, the hyperfine structure must be well understood to develop a spatially resolved diagnostic technique capable of ion flow and temperature measurements. Previous work investigated the lineshape of the transition between the $^5D_4^\circ$ and $^5P_3^\circ$ states of singly-ionized atomic iodine (I II) with laser induced fluorescence (LIF), but the hyperfine structure of the transition was unresolved in those measurements [Steinberger and Scime, Journal of Propulsion and Power, 34, 2018]. In this work, an intermodulated LIF technique is used to measure an enhanced lineshape of the same I II transition. A linear least squares fitting algorithm is used to fit the transition lineshape, where hyperfine transition locations and theorized relative amplitudes are constrained by theory. A lineshape model that incorporates hyperfine transition amplitude enhancement introduced from an intermodulated laser technique is implemented into the fitting function, as well as a nonlinear laser saturation effect. We report converged hyperfine coupling coefficients for these I II states.

© 2021 Elsevier Ltd. All rights reserved.

1. Introduction

The spectrum of singly ionized atomic iodine (I II) has been a topic of scientific investigations dating back to the 1930s when Lacroute [1] and Murakawa [2,3] studied the spectra of I II. classified the hyperfine structure of many of the transitions, and determined the nuclear spin of iodine to be 5/2. Those studies were expanded upon by Martin and Corliss [4] with a broad survey of nearly 2400 I II fine structure transitions observed in electrodeless lamp discharges, though Martin and Corliss did not report measurements of the hyperfine structure. A decade later, molecular iodine was investigated using a intermodulated saturated spectroscopy technique [5]. Radiative lifetime measurements of the excited states were provided by Kono and Hattori [6]. Additional investigations of I II spectra have focused on developing better models of the absorption spectrum of large atoms and ions as well as on applications in optogalvanic instruments and electric propulsion [7-16].

Hargus et al. [13] examined a variety of hyperfine transitions of I II and proposed several transitions appropriate for laser induced fluorescence (LIF) measurements. Using LIF, Steinberger and

* Corresponding author.

E-mail address: mjl0018@mix.wvu.edu (M.J. Lazo).

Scime [15] validated one of those transitions, from the metastable ${}^5D_0^{\circ}$ state to the 5P_3 state, and observed a clear hyperfine structure in the measured lineshape. However, those measurements lacked sufficient resolution to precisely determine the magnetic dipole and electric quadrupole hyperfine coupling coefficients. The hyperfine structure of multiple I II transitions in the range of 12,000–24,000 cm $^{-1}$, which includes the transition studied by Steinberger and Scime, was catalogued by Ashok et al. [17] using Fourier transform spectroscopy. We note that the magnetic dipole and electric quadrupole hyperfine coupling coefficients they report for the ${}^5D_4^{\circ}$ to 5P_3 transition yield a lineshape very different from what is reported in this work. A direct comparison of measured lineshapes for the ${}^5D_4^{\circ}$ to 5P_3 transition is not possible as the measured lineshape itself is not provided in that work.

Here, we provide direct measurements of the lineshape of the $^5D_4^\circ$ to 5P_3 transition in I II using an intermodulated LIF technique. The existence of the hyperfine structure in the transition is clear and the intermodulated LIF technique provides enough resolution to suggest sets of values of the magnetic dipole and electric quadrupole hyperfine coupling coefficients. The remainder of this work is organized as follows. Section 2 describes traditional LIF and the necessity for a modified technique as a result of broadening of the hyperfine transition lineshape. Section 3 details the experimen-

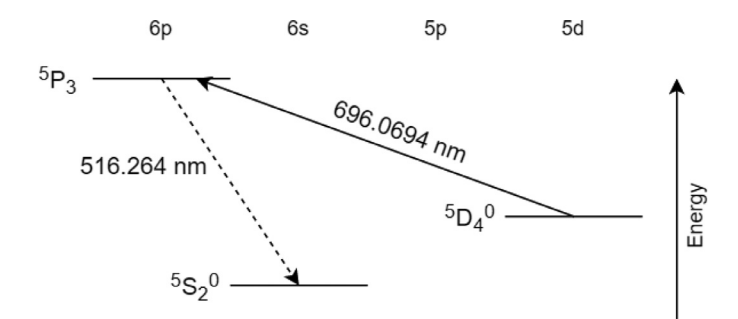


Fig. 1. LIF scheme for the singly ionized atomic iodine transition probed in this work. The pump transition to the metastable excited state is shown by the solid line, and the fluorescent transition to the lower state is shown by the dashed line.

tal configuration. Results are presented in Section 4. Finally, a brief summary is given in Section 5.

2. Laser induced fluorescence

LIF is a non-perturbative absorption spectroscopic technique first introduced in plasmas by Stern and Johnson [18]. LIF uses a specific wavelength of light to excite an electronic transition of an atom or ion, commonly from a metastable state to a higher energy state. As the electron relaxes from the excited state to a lower energy state, a photon is emitted and collected as LIF signal. In a plasma, the particles will possess some random thermal motion which causes a Doppler-shift in the laboratory reference frame transition frequency. As a result, the measured lineshape is broadened around the rest absorption frequency. When the particle motion is purely thermal in nature, the measured lineshape is a convolution of a Maxwellian lineshape (a thermal contribution) and a Lorentzian lineshape (a non-thermal contribution). In a Doppler limited regime, the non-thermal, homogenous lineshape can have a spectral width of hundreds of MHz. The ability of LIF to measure ion velocity distribution functions (IVDFs) makes it a viable diagnostic for non-perturbatively measuring iodine ion flow, ion temperature, and relative state density in a thruster using iodine as its propellant.

The LIF scheme investigated here for I II was first proposed by *Hargus* et al., [13] who performed initial investigations with passive emission spectroscopy, and later validated by *Steinberger and Scime* [15]. Laser light tuned to 696.0964 nm (vacuum) excites the metastable $^5D_4^{\circ}$ state to the 5P_3 upper state, which then decays to the $^5S_2^{\circ}$ state, emitting a photon of wavelength 516.264 ± 0.001 nm [15]. A partial Grotrian diagram of the LIF scheme used in this work is shown in Fig. 1.

2.1. Hyperfine structure of singly ionized atomic iodine

An atom's spectrum of electronic energy levels is naturally split into a fine structure by spin-orbit coupling and relativistic corrections to bound electron orbital motion. The interactions between the nuclear magnetic dipole and electric quadrupole moments cause hyperfine splitting of electronic states [19]. The presence of isotopes also causes hyperfine splitting due to differences in the nuclear mass and spin. However, the only naturally-occurring isotope of iodine is I¹²⁷, which allows the hyperfine structure of the transition probed here to be parameterized solely in terms of the magnetic dipole and electric quadrupole interactions for the upper and lower states [13,15].

When describing the hyperfine structure of an atom, it is convenient to work in the basis which couples the interactions between orbiting electrons and the nucleus. In this basis, the nuclear spin of iodine, I = 5/2, is added to the total electronic angular momen-

tum J of each state, to yield the total angular momentum for each hyperfine state, F [15,19]. Both the ${}^5D_3^{\circ}$ and 5P_3 states are split into 2I+1=6 hyperfine states, each with a unique F, which take on values of $F=I+I,I+I-1,\ldots,|I-I|$ [13].

Each hyperfine state is shifted in energy from the original state as described by

$$\Delta E/h = \Delta v = \frac{A}{2}C + \frac{B}{4} \frac{\frac{3}{2}C(C+1) - 2I(I+1)J(J+1)}{I(2I-1)J(2J-1)}$$
(1)

where h is Planck's constant, C = F(F+1) - I(I+1) - J(J+1), A is the magnetic dipole coupling coefficient, and B is the electric quadrupole coupling coefficient. Following the selection rule $\Delta F = 0, \pm 1$, the original transition is a composition of 15 allowed hyperfine transitions. Table 1 lists each transition and their respective Casimir coefficients, as well theorized relative intensities calculated from Russell-Saunders coupling. The numerical values of the energy shifts for each split state cannot be calculated until the coupling coefficients for the upper and lower states are known [13]. For quick reference, we label the upper state's coupling coefficients as A_U and B_U , and the lower state's coupling coefficients as A_L and B_L . These values are typically determined experimentally.

The overall measured lineshape is modelled by the function

$$f(\nu) = a + b \sum_{i=1}^{i=15} \left(\frac{I_{\circ,i}}{1 + I_{\circ,i}/I_{\text{sat}}} \right)$$

$$\left(\exp\left[-\gamma \frac{(\nu - \nu_{\circ}' - \nu_{hf,i})^{2}}{T_{\text{Dp}}} \right] + c \frac{\left(\frac{1}{2}\Gamma_{\text{int}}\right)^{2}}{(\nu - \nu_{\circ}' - \nu_{hf,i})^{2} + \left(\frac{1}{2}\Gamma_{\text{int}}\right)^{2}} \right)$$
(2)

where a is a DC offset from detecting electronics, b is a global amplitude, $I_{o,i}$ is the theorized relative amplitude of the *i*th hyperfine transition, $I_{\rm sat}$ is a saturation intensity, ν is the relative scanning frequency of the laser, in GHz, $\gamma=\frac{mc^2}{4k\nu_{\circ}}$, with the mass m of I II in kg, the speed of light c in m/s, Boltzmann's constant k in J/K, and ν_{\circ} is the predicted rest frequency of the unsplit transition, ν_{\circ}' is a global frequency offset that accounts for errors in absolute wavelength tabulation, in GHz, $\nu_{hf,i}$ is relative transition center of the ith hyperfine transition in GHz and is a function of the hyperfine coupling coefficients (A_U , A_L , B_U , B_L), T_{Dp} is an effective ion temperature of the Doppler pedestal, c provides the ratio of the intermodulated Lorentzian amplitude to the strongest Maxwellian hyperfine transition (i.e., 1), and Γ_{int} is the spectral width of the narrow, Lorentzian intermodulated contribution of the measured lineshape. In Eq. (2), $I_{o,i}/(1+I_{o,i}/I_{sat})$ is a nonlinear saturation effect [20] of the hyperfine transition amplitudes. The saturation effect described in Ref. [20] is strictly only correct for applications to Zeeman-split subcomponents, but is applied to hyperfine components as a suitable approximation and is incorporated into the analysis in this work. For very strong saturation, $I_{\text{sat}} \rightarrow 0$, and for little to no saturation, $I_{\text{sat}} \rightarrow \infty$. Intermodulated laser spectroscopy (Section 2.2) enhances signal from particles at or near zero velocity. Specifically, an increase in amplitude at rest frequency is observed in addition to a background Doppler lineshape. To model this effect, a narrow Lorentzian feature is introduced in summation with the Doppler-broadened hyperfine transition, with the amplitude of this feature representing the ratio of the Lorentzian contribution to the Maxwellian contribution. Eq. (2) has a total of 11 free parameters: a, b, I_{sat} , ν'_{\circ} , T_{Dp} , c, Γ_{int} , A_U , A_L , B_U , and B_L . It is noted that contributions from cross-over signals [21] are not accounted for in this model.

2.2. Intermodulated spectroscopy

At the scale of hyperfine structure energy shifts, Doppler broadening observed in traditional LIF results in several overlapping hy-

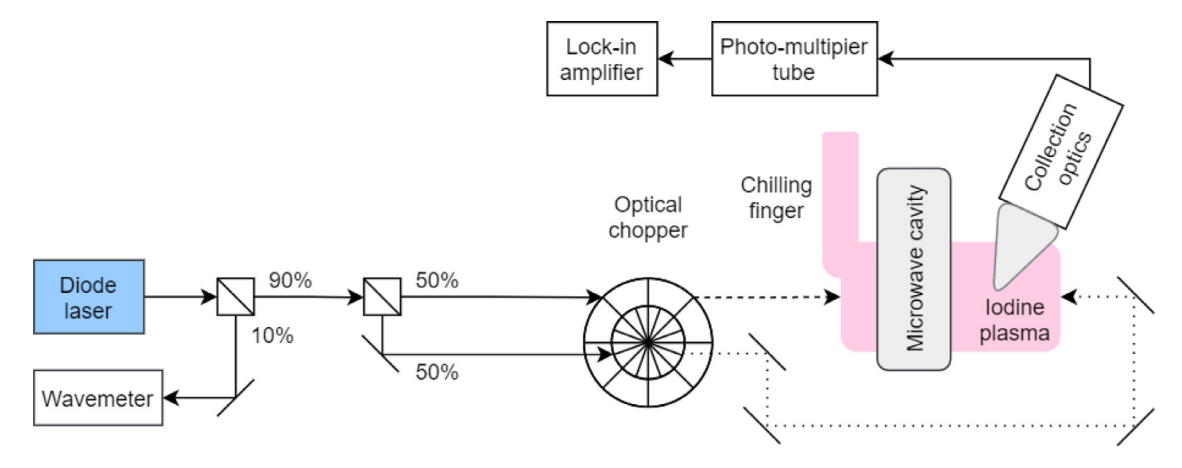


Fig. 2. Diagram of the experimental apparatus. A diode laser beam tuned to 696.0694 nm is monitored with a wavelength meter and sent through a beam splitter which creates two equal intensity beams which are modulated at two different frequencies. The modulated beams are sent antiparallel along the mechanical axis of the quartz iodine cell, exciting iodine ions emitting light which is collected and filtered before being amplified by a photomultiplier tube. The microwave cavity shown is driven at 2.45 GHz and used to maintain the source plasma. The chilling finger is used to regulate the plasma partial pressure.

perfine transitions, which makes it difficult or impossible to resolve individual hyperfine transitions. This was clearly evident in the initial LIF measurements of I II [15]. Therefore, an intermodulated LIF technique [5,22,23] is implemented to better resolve each of the 15 hyperfine transitions probed in this work.

Intermodulated spectroscopy intersects two laser beams from the same source at a point in the plasma, with each beam modulated at a frequency which is not a harmonic of the other. The total LIF signal at the sum of the two modulation frequencies is recorded. In this technique, ions at or near zero velocity see an increase in laser intensity at the sum frequency, enhancing the signal from particles at rest and reducing the effective Doppler width of the measured lineshape. While this technique is referred to as "Doppler-free" in literature, it does not generally produce a true Doppler-free lineshape since the signal is also enhanced from particles with equal magnitude, oppositely directed velocities that simultaneously interact with the individual laser beams. A "Doppler pedestal" created from velocity-changing collisions has also been observed [24] and is characterized by $T_{\rm Dp}$ in Eq. (2) The net effect is an enhancement in the emission at the rest frame transition because of the larger number of rest ions compared to ions in motion. Therefore, the lineshapes presented in this work are enhanced around zero velocity and show clear hyperfine peaks compared to the traditionally measured I II lineshape.

3. Experimental configuration

Figure 2 shows a diagram of the experimental configuration for the measurements presented here. The plasma source consists of a crystalline iodine sample sealed within an Opthos Instruments Inc. quartz cell at $< 10^{-4}$ Torr [15]. The cell is kept stationary and partially inserted into an Evenson microwave resonant cavity which is driven at 2.45 GHz. Extending from the cell is a chilling finger through which an equal-parts mixture of ethylene glycol and water is circulated by a Polyscience PD07R-40 chiller that has an operating range of -20° C to 100° C. Kono and Hattori [6] measured the iodine partial pressure in a similar cell configuration to be

$$\log_{10}(P) = 18.8 - 3594/T_{cf} + 0.00044T_{cf} - 2.98\log_{10}(T_{cf}), \quad (3)$$

where P is in torr and T_{cf} is the chilling finger temperature in degrees Kelvin, therefore, the internal pressure is controlled via the chilling finger temperature. The source was operated between -15° C and $+5^{\circ}$ C (6.4 - 52 mTorr) for this work.

A Toptica Photonics DL Pro single-mode diode laser was tuned to the transition wavelength and split such that 10% of the beam

was directed into a Wavemeter WA-1500 laser wavelength meter for realtime wavelength monitoring. The wavelength meter has an accuracy of ± 0.1 pm [25]. The remaining 90% of the beam is coupled into a $\varnothing 5~\mu m$ single mode optical fiber and passed through a second beam splitter, sending two 50% beam components through a chopper with two different fin spacings. The two beams are modulated such that their sum frequency is 7.1 kHz. The beams are then redirected into the source antiparallel along the mechanical $(\hat{z}-)$ axis of the cell. Light emitted from the cell was captured by a set of collection optics and a $\varnothing 1$ mm multi-mode fiber optic cable. Collected light is detected with a Hamamatsu HC120-05MOD photomultiplier tube. Spontaneous emission is distinguished from the desired LIF emission using a Stanford Research SR830 lock-in amplifier referenced to the sum of the two chopping frequencies.

4. Results

Figure 3 shows a side by side view of typical I II lineshape measurements performed with traditional LIF and intermodulated LIF. Both were measured in the same plasma configuration described in Section 3. For both spectroscopic approaches, the souce was operated at 6.4 mTorr. For the traditional LIF measurement (a), a time-averaged laser power of ~ 1.54 mW was injected; for the intermodulated measurement (b), time-averaged laser powers of 1.50 and 1.54 mW were injected for each beam, respectively. The frequency axis of these measurements is uncalibrated, but is shown to highlight the enhancement of the lineshape when using the intermodulated LIF technique.

In an investigation into the hyperfine structure of niobium I with LIF, Faisal et al. [20] introduced a laser saturation effect, originally applied to Zeeman-split subcomponents, to their hyperfine structure analysis. This effect is a nonlinear mechanism capable of altering the relative amplitudes of individual hyperfine transitions in a measured lineshape. In the present investigation, this effect is approximated by applying the saturation formula to the intensities of the hyperfine components (see Eq. (2)). Strong saturation also introduces an artificial broadening to a measured lineshape. To determine if the measurements here are strongly influenced by laser saturation, the overall measured spectral width of the probed transition was evaluated as a function of instantaneous injected laser power, which was varied from ~ 1 mW to ~ 5 mW. Figure 4 shows no observable dependence of the overall measured spectral width on injected laser intensity, and therefore this effect is expected to be small for the measurements presented in this work, but is included in Eq. (2) for completeness.

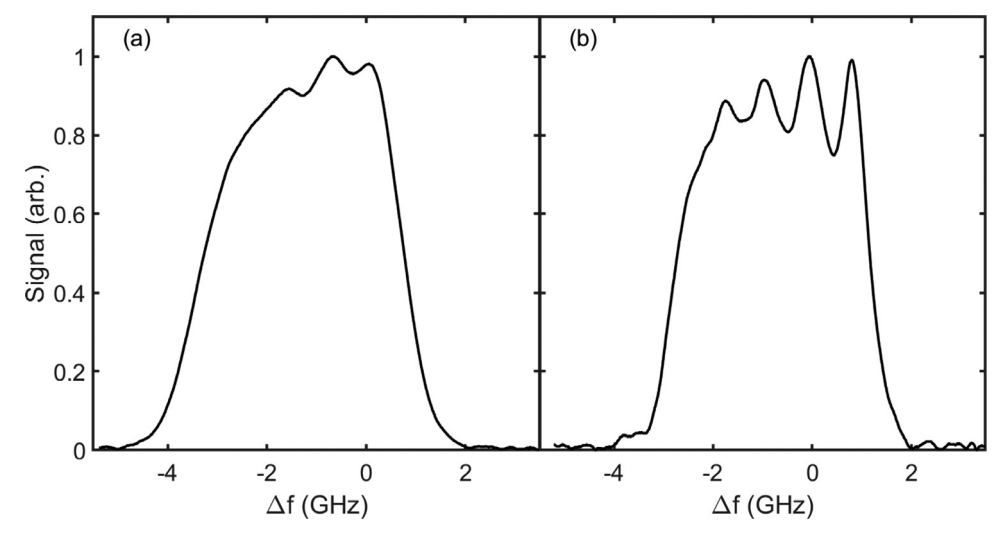


Fig. 3. Side by side comparison of a typical I II lineshape measured with traditional LIF (a) and the intermodulated technique (b) described in Section 3. While the frequency shown in this plot has an uncalibrated offset, the enhancement of the hyperfine structure in (b) is apparent.

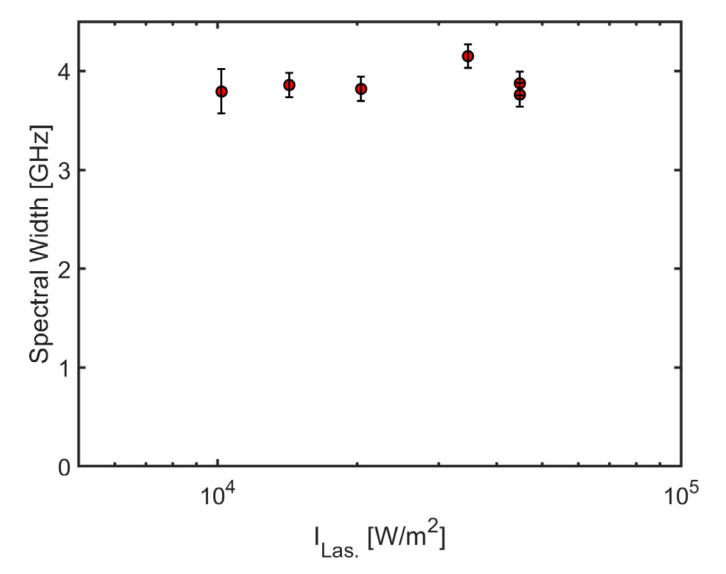


Fig. 4. Spectral width, in GHz, as a function of injected laser intensity, in W/m², for six different intermodulated LIF measurements. Injected powers ranged from ~ 1 mW to ~ 5 mW. The invariance of the spectral width across the range of injected laser intensities suggests that power saturation effects are small in this investigation

Figure 5 shows a fit of Eq. (2) (red-dashed line) to an I II line-shape measured with intermodulated LIF (solid black line). The root mean squared error associated with this fit is 0.012, suggesting a near "excellent" fit [26]. The location of each hyperfine transition with the respective transition relative amplitude is shown by the vertical black dashed lines. Under each transition is the corresponding transition number from Table 1. The hyperfine coupling coefficients and ion temperature of the Doppler pedestal are determined from this fit and are shown in Table 2 along with the intermodulated amplitude contribution, the saturation parameter, the ion temperature, and the spectral width of the narrow intermodulated feature.

It should be noted that slight changes in initial guesses for each free parameter in Eq. (2) converge to equally impressive fits to the I II lineshape, but with different hyperfine coefficients. However, the magnitudes of difference between the magnetic dipole and electric quadrupole coefficients remain approximately constant, suggesting that the difference between the hyperfine coefficients of the upper

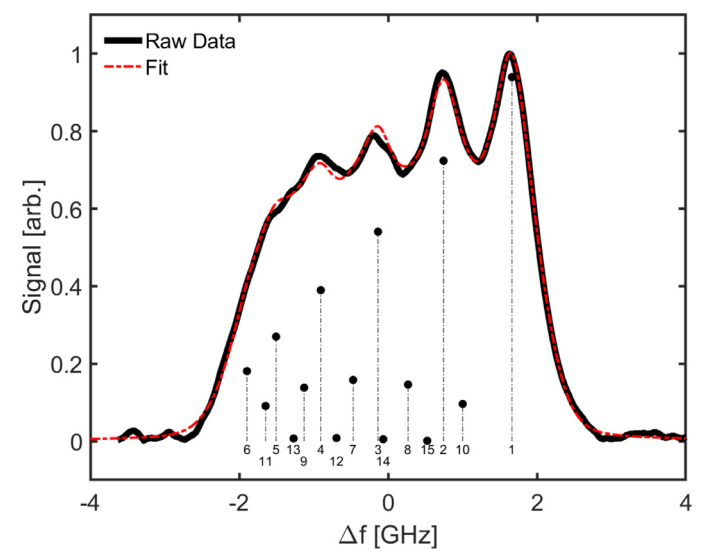


Fig. 5. Linear least squares fit (red dashed line) to an I II lineshape measured with intermodulated LIF (black solid line). Intermodulated LIF introduces an enhancement in amplitudes at hyperfine transition rest frequencies and is modeled in the fit function. A ratio of the unsaturated strongest hyperfine transition to the saturation intensity of $I_{\circ,1}/I_{\rm sat}\approx 1/17$ is determined from the fit results, suggesting weak saturation. (For interpretation of the references to color in this figure legend, the reader is referred to the web version of this article.)

and lower state of the probed transition is what determines the hyperfine splitting magnitude rather than the absolute values of the hyperfine coefficients.

Using the values for the hyperfine coefficients determined from the intermodulated technique, a fit to a traditionally measured iodine lineshape was performed for an iodine operating pressure of ~ 50 mTorr and a microwave power of $P_{\rm MW} = 30$ W. Figure 6 shows the fit (red dashed line) to a lineshape measured with nonintermdodulated, traditional LIF (solid black line). The hyperfine coefficients from Table 2 describe the non-intermodulated lineshape well and a reliable ion temperature is determined. For this measurement, the ion temperature is $T = 0.127 \pm 0.002$ eV, consistent with xenon ion measurements in similar discharges [27]. Hyperfine transition locations and relative amplitudes are shown by the dashed black lines. Similar to Fig. 5, under each transition is the corresponding transition number from Table 1. The narrow fea-

Table 1
Table of allowed hyperfine transitions between the lower ${}^5D_4^{\circ}$ and upper 5P_3 states. The frequency difference between the lower and upper hyperfine state in each transition is given by $\Delta v_{hf,i}$ in terms of the coupling coefficients, generating a system of 15 equations and 19 unknown quantities. Transition numbers in the leftmost column are correlated with their derived locations in Fig. 5. The theorized relative intensities, calculated from Russell-Saunders coupling, are included in the rightmost column.

Transition	$F_L o F_U$	$\Delta v_{hf,i}(A_U, B_U, A_L, B_L)$	Relative Intensity
1	13/2 → 11/2	$\Delta v_{hf,1} = 7.5 A_U + 0.25 B_U - 10 A_L - 0.25 B_L$	100.000
2	$11/2 \rightarrow 9/2$	$\Delta v_{hf,2} = 2A_U - 0.3B_U - 3.5A_L + 0.2375B_L$	75.974
3	$9/2 \rightarrow 7/2$	$\Delta v_{hf,3} = -2.5 A_U - 0.3 B_U + 2 A_L + 0.29643 B_L$	56.122
4	$7/2 \rightarrow 5/2$	$\Delta v_{hf,4} = -6A_U - 0.02B_U + 6.5A_L + 0.10357B_L$	40.087
5	$5/2 \rightarrow 3/2$	$\Delta v_{hf,5} = -8.5 A_U + 0.334 B_U + 10 A_L - 0.19643 B_L$	27.551
6	$3/2 \rightarrow 1/2$	$\Delta v_{hf6} = -10A_U + 0.6B_U + 12.5A_L - 0.49107B_L$	18.367
7	$7/2 \rightarrow 7/2$	$\Delta v_{hf7} = -2.5 A_U - 0.3 B_U + 6.5 A_L + 0.10357 B_L$	16.035
8	$9/2 \rightarrow 9/2$	$\Delta v_{hf,8} = 2A_U - 0.3B_U + 2A_L + 0.29643B_L$	14.842
9	$5/2 \rightarrow 5/2$	$\Delta v_{hf,9} = -6A_U - 0.02B_U + 10A_L - 0.19643B_L$	13.994
10	$11/2 \to 11/2$	$\Delta v_{hf,10} = 7.5 A_U + 0.25 B_U - 3.5 A_L + 0.2375 B_L$	9.740
11	$3/2 \rightarrow 3/2$	$\Delta v_{hf 11} = -8.5 A_U + 0.334 B_U + 12.5 A_L - 0.49107 B_L$	9.184
12	$5/2 \rightarrow 7/2$	$\Delta v_{hf,12} = -2.5A_U - 0.3B_U + 10A_L - 0.19643B_L$	1.312
13	$3/2 \rightarrow 5/2$	$\Delta v_{hf,13} = -6A_U - 0.02B_U + 12.5A_L - 0.49107B_L$	1.020
14	$7/2 \rightarrow 9/2$	$\Delta v_{hf,14} = 2A_U - 0.3B_U + 6.5A_L + 0.10357B_L$	1.020
15	$9/2 \rightarrow 11/2$	$\Delta v_{hf,15} = 7.5 A_{IJ} + 0.25 B_{IJ} + 2 A_{L} + 0.29643 B_{L}$	0.464

Table 2Values derived from a linear least squares fit of the I II lineshape. Uncertainty in each value is represented by a 95% confidence interval produced from the fit. It is seen that all parameters are well constrained by this technique. It should be noted that slight changes in initial guesses produce equally good fits with differing hyperfine coefficients. However, differences between the magnetic dipole and electric quadrupole coupling coefficients for each state remain approximately constant.

Parameter	Value	
A _U (MHz)	89.8 ± 4.6	
A_L (MHz)	-84.2 ± 3.5	
B_U (MHz)	-430.0 ± 37.6	
B_L (MHz)	-233.8 ± 44.0	
$I_{\circ,1}/I_{sat}$	1/17	
c	0.41	
$T_{\rm Dp}$ (eV)	0.084 ± 0.002	
$\Gamma_{\rm int}$ (MHz)	506.6 ± 31.0	

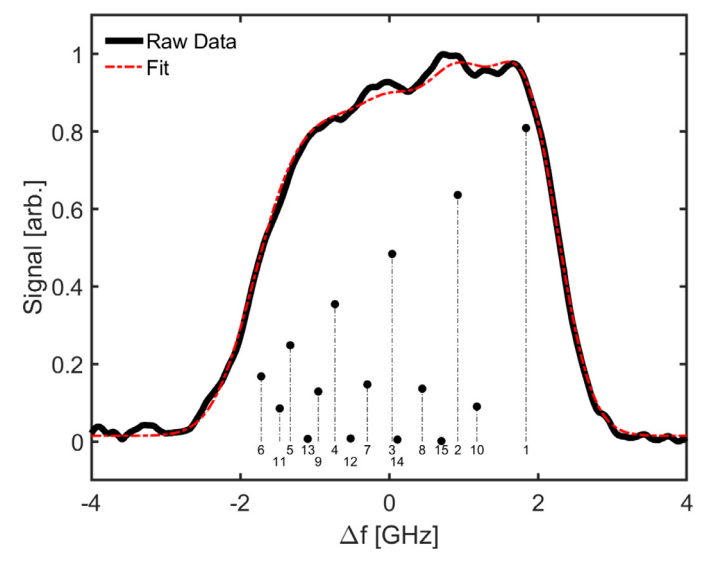


Fig. 6. Linear least squares fit (red dashed line) to an I II lineshape measured with traditional LIF (black solid line). The predetermined hyperfine coeffecients are sufficient to describe the measured lineshape with only modest adjustment of the ion temperature. Hyperfine transition locations and relative amplitudes are indicated by the dashed black lines with transition number corresponding to Table 1 shown under each transition. (For interpretation of the references to colofr in this figure legend, the reader is referred to the web version of this article.)

ture introduced in Eq. (2) to account for intermodulated amplitude is not included when fitting to a traditionally measured lineshape.

5. Conclusions

An intermodulated laser induced fluorescence technique is demonstrated to resolve an enhanced lineshape of singly-ionized atomic iodine within a microwave plasma discharge. The hyperfine structure of the $^5D_4^{\circ}$ and 5P_3 states is analyzed and possible values for the magnetic dipole and electric quadrupole coupling coefficients are derived from a fit of the modeled lineshape to the measured lineshape. Here we have incorporated a narrow feature into the modeled lineshape to account for amplitude enhancements introduced from an intermodulated LIF technique. The derived hyperfine coefficients are also well-suited to describe an I II lineshape measured with traditional LIF. With knowledge of these parameters, measurements of iodine ion temperatures and bulk flows are achievable, providing a viable non-perturbative laser spectroscopic technique to investigate electric thrusters using iodine as a propellant.

Declaration of Competing Interest

The authors declare that they have no known competing financial interests or personal relationships that could have appeared to influence the work reported in this paper.

CRediT authorship contribution statement

M.J. Lazo: Software, Validation, Formal analysis, Investigation, Resources, Data curation, Writing – original draft, Writing – review & editing, Visualization. **T.E. Steinberger:** Conceptualization, Methodology, Software, Validation, Formal analysis, Investigation, Resources, Writing – review & editing, Supervision, Project administration. **T.N. Good:** Conceptualization, Methodology, Writing – review & editing. **E.E. Scime:** Conceptualization, Resources, Writing – review & editing, Supervision, Funding acquisition.

Acknowledgements

The authors would like to thank Dr. William A. Hargus, Jr., of the Edwards Air Force Research Laboratory, as well as Dr. William Amatucci, and the Naval Research Laboratory for providing several key pieces of the experimental apparatus for this work. We would additionally like to thank Mitchell Paul and Dr. Peiyun Shi for technical consultations. This work was supported by the West Virginia University Center for KINETIC Plasma Physics.

References

- [1] Lacroute P.. Effet zeeman du bromine et de l'iode. 1934.
- [2] Murakawa K. Anomalies in the fine structure of the first spark spectrum of iodine. Nature 1936;137(3477):1030–1.
- [3] Murakawa K. Quadrupole coupling in the hyperfine structure of the spectrum of I II. | Phys Soc |pn 1964;19(9):1539–41.
- [4] Martin WC, Corliss CH. The spectrum of singly ionized atomic iodine (I II). J ResNatl BureauStand. 1960;64A(6).
- [5] Sorem MS, Schawlow AL. Saturation spectroscopy in molecular iodine by intermodulated fluorescence. Opt Commun 1972;5(3):148–51. doi:10.1016/ 0030-4018(72)90053-3.
- [6] Kono A, Hattori S. Radiative-lifeteime measurements for I I and I II. J Opt Soc Am 1979;69(2):253–5.
- [7] Szabo J, Robin M, Paital S, Pote B, Hruby V, Freeman C. Iodine propellant space propulsion. In: Proceedings of the 33rd international electric propulsion conference; 2013. IEPC-2013-311.
- [8] Dressler R, Chiu Y-H, Levandier DJ. Propellant alternatives for ion and hall effect thrusters. 38th Aerospace sciences meeting and exhibit; 2000. AIAA Paper 2000-0602. doi:10.2514/6.2000-602.
- [9] Szabo J, Pote B, Paital S, Robin M, Hiller A, Branam RD, et al. Performance evaluation of an iodine-vapor hall thruster. J Propul Power 2012;28(4):848–57. doi:10.2514/1.B34291.
- [10] Linnell JA, Gallimore AD. Efficiency analysis of a hall thruster operating with krypton and xenon. J Propul Power 2006;22(6):1402–18. doi:10.2514/1.19613.
- [11] Jacobson D, Manzella D. 50 kw class krypton thruster performance. 39th AIAA/ASME/ASEE joint propulsion conference and exhibit; 2003. AIAA Paper 2003-4550. doi:10.2514/6.2003-4550.
- [12] Tverdokhlebov O, Semenkin A. Iodine propellant for electric propellant to be or not to be. 37th Joint propulsion conference and exhibit; 2001. AIAA Paper 2001–3350. doi:10.2514/6.2001-3350.
- [13] Hargus W, Lubkeman J, Remy K, Gonzales A. Investigation of singly ionized iodine spectroscopy in support of electrostatic propulsion diagnostics development. 48th AIAA/ASME/SAE/ASEE joint propulsion conference and exhibit; 2012. doi:102514/62012-4316.

- [14] Duchemin O, Valentian D, Cornu N. Cryostorage of propellants for electric propulsion. Proceedings of the 45th joint propulsion conference and exhibit; 2009. AIAA Paper 2009-4912. doi:10.2514/6.2009-4912.
- [15] Steinberger T, Scime E. Laser-induced fluorescence of singly ionized iodine, J Propul Power 2018;34(5):1235–9. doi:10.2514/1.B37107.
- [16] Hiller AC. Revolutionizing space propulsion through the characterization of iodine as fuel for hall-effect thrusters. Air Force Institute of Technology, Wright-Patterson AFB; 2011. Master's thesis.
- [17] Ashok C, Vishwakarma SR, Deo MN. Hyperfine structure measurements on singly ionized atomic iodine (I II) using fourier transform spectroscopy. J Quant Spectrosc Radiat Transf 2018;221:71–9.
- [18] Stern RA, Johnson JAI. Plasma ion diagnostics using resonant fluorescence. Phys Rev Lett 1975;34(1548). doi:10.1103/PhysRevLett.34.1548.
- [19] McIntyre DH. Quantum mechanics: a paradigms approach. 2nd ed. Pearson Addison-Wesley; 2012. ISBN 978-0-321-76579-6.
- [20] Faisal M, Windholz L, Kröger S. Systematic investigations of the hyperfine structure constants of niobium I levels. Part I: constants of upper odd parity energy levels between 16,672 and 31,025 cm⁻¹ and discovery of a new level. I Ouant Spectrosc Radiat Transf 2020;245. doi:10.1016/j.igsrt.2020.106873.
- [21] Foot C. Atomic physics. Oxford Master Series in Physics. Oxford University Press; 2005. ISBN 9780198506959.
- [22] Lawler JE, Ferguson AI, Goldsmith JEM, Jackson DJ, Schawlow AL. Doppler-free intermodulated optogalvanic spectroscopy. Phys Rev Lett 1979;42(16):1046–9. doi:10.1103/PhysRevLett.42.1046.
- [23] Luo P-L, Hu J, Feng Y, Wang L-B, Shy J-T. Doppler-free intermodulated fluorescence spectroscopy of 4he 23p-31,3d transitions at 588 nm with a 1-w compact laser system. Appl Phys B 2015;120(2):279-84. doi:10.1007/s00340-015-6135-8.
- [24] Thornton DE, Phillips GT, Perram GP. Velocity changing collisions in the laser saturation spectra of 87rb d2 f=2,. Opt Commun 2011;284(12):2890-4. doi:10. 1016/j.optcom.2011.02.057.
- [25] EXFO Electro-Optical Engineering Inc.. Use Guide: WA-1000/WA-1500 Wavemeter Laser Wavelength Meters; 2004.
- [26] MacCallum RC, Browne MW, Sugawara HM. Power analysis and determination of sample size for covariance structure modeling. Psychol Methods 1996;1(2):130–49.
- [27] Smith TB, Ngom BB, Linnell JA, Gallimore AD. Diode laser induced fluorescence of xenon ion velocity distributions. 41st AIAA/ASME/SAE/ASEE joint propulsion conference and exhibit. American Institute of Aeronautics and Astronautics paper 2005-4406; July 2005. doi:102514/62005-4406.